Geochemical Perspectives Letters

Published by the European Association of Geochemistry

Final assembly of Gondwana enhances crustal metal (HREE and U) endowment

P. Liu[1,2*], S.A. Gleeson[2,3], N.J. Cook[4], B. Lehmann[5], C. Zhao[6], W. Yao[1], Z.A. Bao[1], S.T. Wu[7], Y.F. Tian[8], J.W. Mao[8]

Abstract

https://doi.org/10.7185/geochemlet.2317

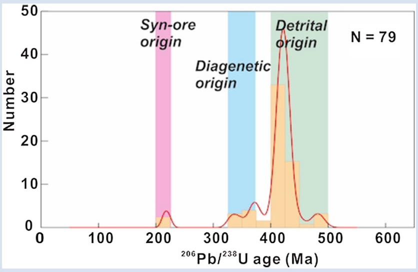

The South China Block hosts a variety of U and HREE mineralisation styles. The Yushui Cu deposit is located at a sedimentary unconformity and is enriched in HREEs and U. U-Pb ages of uraninite and xenotime indicate that the HREE mineralisation is epigenetic and formed at *ca.* 223 ± 1 Ma. Ore petrography, elemental mapping, and Nd isotope data suggest that HREEs and U were leached from the footwall sandstone and transported to the Cu deposit *via* oxidised basinal brines. U-Pb ages of detrital xenotime and zircon from the sandstone show that this sedimentary sequence was mainly derived from Silurian S-type granites, which were emplaced during Gondwana amalgamation. Rapid erosion formed clastic sedimentary rocks that contain accessory HREE-U minerals which could be remobilised by younger mineralising events. S-type granite magmatism during the final assembly of Gondwana established the crustal metal reservoir which was repeatedly tapped over geological history, including the modern formation of regolith hosted HREE deposits in South China. Given the global distribution of analogous S-type granites in other terranes globally, our study has exploration implications outside of China. This will be enlightening for finding new HREE deposits, which is vital to support the transition to a low carbon footprint energy.

Received 13 March 2023 | Accepted 3 May 2023 | Published 26 May 2023

Introduction

Genetic relationships between ore formation and crustal evolution are long established (Sawkins, 1984; Cawood and Hawkesworth, 2015). These relationships may, however, be difficult to identify due to the interplay between multiple geological processes (*e.g.*, magmatism, sedimentary processes, and weathering) and the complexity of crustal evolution. Sediment hosted ore deposits commonly display evidence for a protracted sequence of mineralising events stretching from sedimentation to diagenesis to post-diagenetic metamorphism and/or metasomatism (Hitzman *et al.*, 2005). Thus, these systems can help elucidate the relationship between ore formation and crustal evolution.

Although detrital zircon U-Pb geochronology of clastic sedimentary rocks is a well established tool for reconstructing crustal evolution (Košler *et al.*, 2002), xenotime U-Pb geochronology provides a unique glimpse into not only sedimentary sources (*e.g.*, detrital xenotime; Kositcin *et al.*, 2003) but also into the post-depositional history of the sedimentary sequences (*e.g.*, diagenetic xenotime; McNaughton *et al.*, 1999). Xenotime is a widespread heavy rare earth (HREE) mineral which can form by magmatic, sedimentary, and hydrothermal processes but typically has small grain sizes (<20 μm); this has previously hampered routine U-Pb dating of xenotime. However, recent advances in microanalytical *in situ* U-Pb dating methods have improved the spatial resolution (~10 μm) achievable by laser ablation inductively coupled plasma mass spectrometry (LA-ICP-MS) (Wu *et al.*, 2020). Contemporary microanalysis thus can circumvent the common problem of small grain size (<20 μm) and allows routine U-Pb xenotime dating of clastic sedimentary rocks.

We present *in situ* LA-ICP-MS U-Pb ages for xenotime and uraninite from the Yushui deposit (South China), a sediment hosted high grade Cu deposit. We integrate these data with petrography and Nd isotope data for the footwall sandstone, and propose that the HREEs and U were leached from the red footwall sandstone *via* oxidised basinal brines. The U-Pb dates from clastic xenotime and detrital zircon show that the footwall sandstone is mainly sourced from Silurian S-type granites, which

---

1. State Key Laboratory of Continental Dynamics, Department of Geology, Northwest University, Xi'an 710069, China
2. GFZ German Research Centre for Geosciences, Potsdam 14473, Germany
3. Institute of Geological Sciences, Freie Universität Berlin, Berlin 14463, Germany
4. School of Chemical Engineering, The University of Adelaide, South Australia 5005, Australia
5. Mineral Resources, Clausthal University of Technology, Clausthal–Zellerfeld 38678, Germany
6. School of Earth Science and Resources, Chang'an University, Xi'an 710054, China
7. Institute of Geology and Geophysics, Chinese Academy of Sciences, Beijing 100029, China
8. MNR Key Laboratory for Exploration Theory and Technology of Critical Mineral Resources, China University of Geosciences, Beijing, 100083, China
* Corresponding author (email: pengliu@nwu.edu.cn)

were formed in the South China block when it represented the northern margin of East Gondwana. Given that the amalgamation of Gondwana is the most important period of S-type granite production in geological history, we suggest that the final assembly of Gondwana enhanced crustal metal (HREE and U) endowment in China, but also worldwide. Therefore, similar processes may be important in other S-type granite provinces, a finding that carries significant global implications for rare earth exploration, which can be further pivotal to pursuing a successful green energy transition.

Geological Background and Samples

The Yushui Cu deposit is located in eastern Guangdong Province. The economically important bedded/massive mineralisation is hosted at an unconformity between the lower Carboniferous red sandstone of the Zhongxin Formation and a dark grey dolostone/limestone of the upper Carboniferous Hutian Formation (Fig. S-1). The >300 m thick Zhongxin Formation comprises hematite-bearing red sandstone with abundant detrital minerals including xenotime, rutile, and zircon (Figs. 1b, S-2a–c). The Hutian Formation is predominantly composed of >350 m thick dolomite and limestone with organic- and apatite-rich beds in the lower part (Fig. S-2d). The bedded/massive mineralisation comprises Cu sulfides, barite, hematite, anhydrite, sphalerite, galena (Fig. S-2e,f), and U and HREE-rich minerals, with local HREE grades up to 6.1 wt. % (Fig. S-3, Table S-1). The HREE-rich domains include uraninite (Fig. 1c), hingganite-[Y] ($Y_2Be_2[SiO_4]_2[OH]_2$, Fig. 1d), thortveitite ($[Sc,Y]_2Si_2O_7$, Fig. 1e), jingwenite-[Y] ($Y_2Al_2V^{4+}{}_2[SiO_4]_2O_4[OH]_4$, Fig. 1f; Liu *et al.*, 2023), xenotime (Fig. 1g), iimoriite-[Y] ($Y_2[SiO_4]\,[CO_3]$, Fig. S-4a), synchysite-[Y] ($CaY[CO_3]_2F$, Fig. S-4b), kamphaugite-[Y] ($CaY[CO_3]_2[OH]\cdot H_2O$, Fig. S-4c), and chernovite-[Y] ($Y[AsO_4]$, Fig. S-4d). Samples with hingganite-[Y], uraninite, and xenotime were collected from the bedded/massive mineralisation, and detrital zircon and xenotime were sampled from the lower Carboniferous red sandstone. There are three types of xenotime grains in the sandstone: xenotime-(I) occurring as anhedral grains intergrown with hematite forming veinlets (Fig. S-4e), xenotime-(II) occurring as fine grained (5–15 μm) anhedral grains (Fig. S-4f), and xenotime-(III) occurring as euhedral to subhedral grains intergrown with detrital zircon and quartz (Figs. S-2c, S-4g,h). Sample details are given in Figure S-5; analytical methods in Supplementary Information.

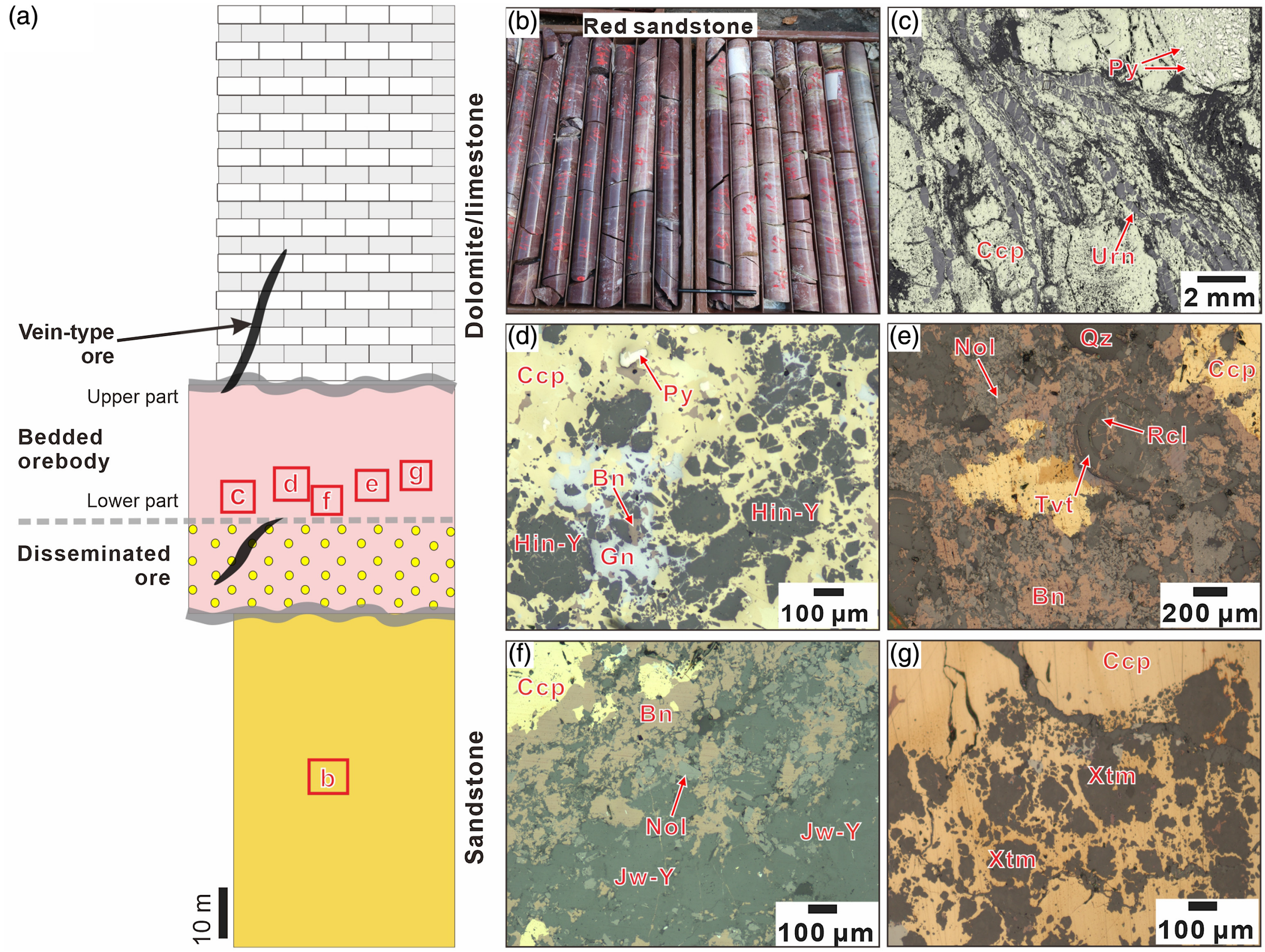

Figure 1 **(a)** Stratigraphic column of the Yushui deposit. **(b)** Photographs of the red sandstone. **(c–g)** Reflected light photomicrographs showing the HREE- and U-bearing minerals from the bedded mineralisation. **(c)** Elongated aggregates of uraninite, **(d)** subhedral hingganite–[Y] grains, **(e)** anhedral roscoelite and colloidal thortveitite, **(f)** agglomerate of euhedral jingwenite–[Y], and **(g)** subhedral xenotime grains in a matrix of bornite and chalcopyrite. Bn, bornite; Ccp, chalcopyrite; Hin–Y, hingganite–[Y]; Gn, galena; Jw–Y, jingwenite–[Y]; Nol, nolanite; Py, pyrite; Qz, quartz; Rcl, roscoelite; Tvt, thortveitite; Urn, uraninite; Xtm, xenotime.

Results

***In situ* U-Pb dating of xenotime, zircon, and uraninite.** Fifty seven spot analyses of 26 uraninite grains yielded a weighted mean ^{206}Pb/^{238}U age of 223.7 ± 0.8 Ma (2σ, MSWD = 0.7) (Fig. 2a, Table S-2). Thirty spot analyses of 25 xenotime grains from the bedded/massive orebody returned a lower intercept age of 221.8 ± 3.5 Ma (2σ, MSWD = 2.2) on a Tera-Wasserburg plot. The ^{207}Pb corrected ^{206}Pb/^{238}U ages yielded a weighted mean of 222.4 ± 2.4 Ma (2σ, MSWD = 1.5) (Fig. 2b, Table S-2).

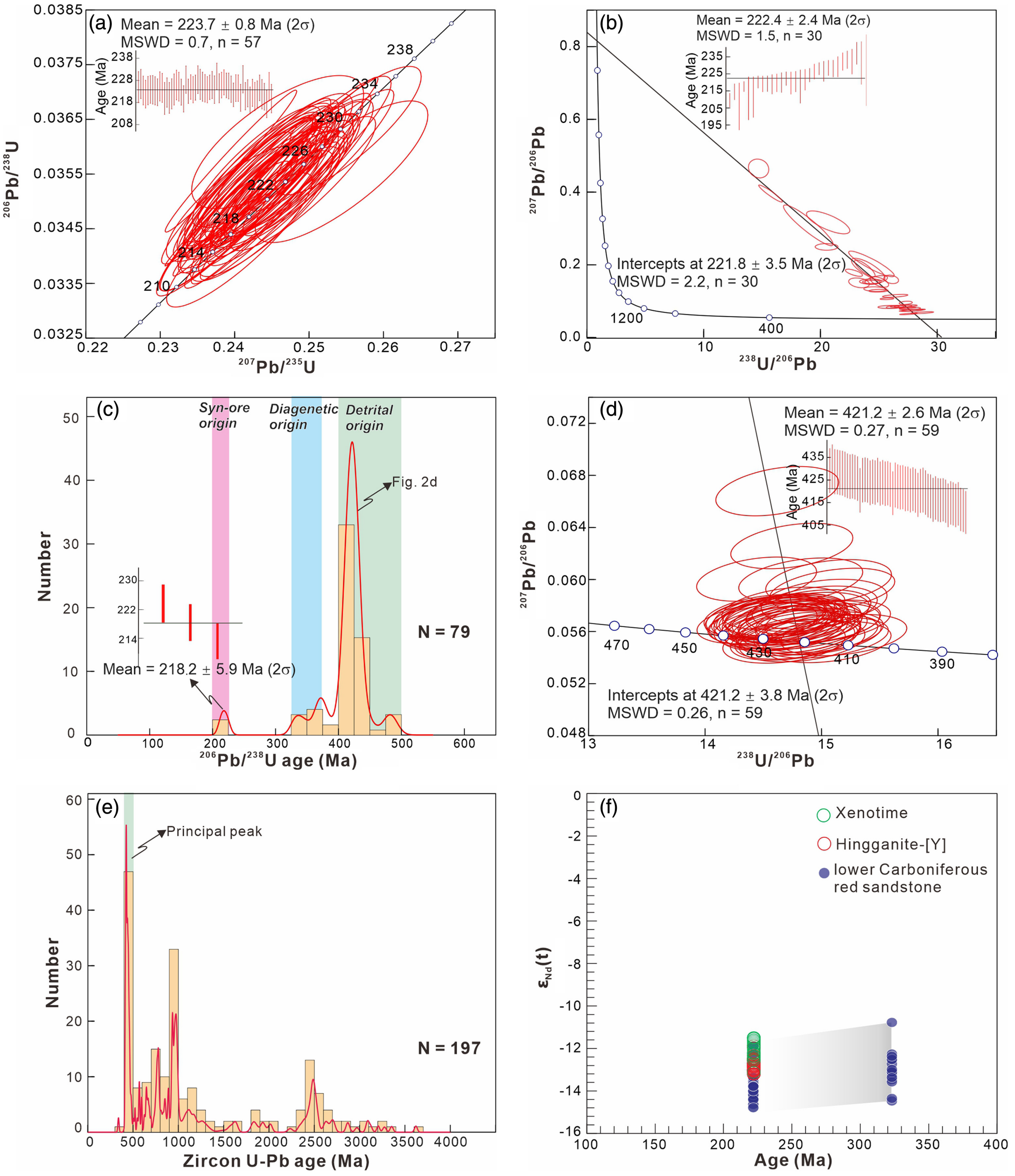

Figure 2 **(a–e)** LA-ICP-MS U-Pb isotope diagrams of **(a)** uraninite and **(b)** xenotime from the bedded mineralisation, **(c, d)** xenotime and **(e)** detrital zircon from the footwall red sandstone. **(c)** and **(d)** show ages for xenotime from the red sandstone. Three spot analyses on xenotime-I yielded a weighted mean age **(c)**, and fifty nine spots on xenotime-III returned a lower intercept age and weighted corrected age **(d)**. **(f)** $\varepsilon_{Nd}(t)$ *vs.* t plot of the red sandstone, and the hingganite-[Y] and xenotime from the bedded mineralisation.

Seventy nine spot analyses of xenotime-I, -II, and -III from the footwall red sandstone yielded three ranges of U-Pb ages at 228–218 Ma ($n = 3$), 387–329 Ma ($n = 11$), and 486–404 Ma ($n = 65$) (Fig. 2c, Table S-3), respectively. Three spot analyses on xenotime-I with the range at 228–218 Ma yielded a weighted mean ^{206}Pb/^{238}U age of 218.2 ± 5.9 Ma. Fifty nine spot analyses on xenotime-III from the major peak at 431–404 Ma returned a lower intercept age of 421.2 ± 3.8 Ma (2σ, MSWD = 0.26) on the Tera-Wasserburg plot, and a ^{207}Pb corrected weighted mean ^{206}Pb/^{238}U age of 421.2 ± 2.6 Ma (2σ, MSWD = 0.27) (Fig. 2d). 197 spot analyses of detrital zircon of the footwall red sandstone yielded three major peaks at 470–410 Ma ($n = 45$), 1100–900 Ma ($n = 42$), and 2600–2300 Ma ($n = 24$) (Fig. 2e, Table S-4).

***In situ* and bulk rock Sm-Nd isotope composition.** Thirty *in situ* spot analyses on 30 hingganite-[Y] grains yielded a Sm-Nd isochron age of 233 ± 12 Ma (2σ, MSWD = 0.8) (Fig. S-6a, Table S-5). Twenty one *in situ* spot analyses on 20 xenotime grains from the orebody returned a Sm-Nd isochron age of 225 ± 26 Ma (2σ, MSWD = 0.19) (Fig. S-6b, Table S-5), similar to the U-Pb age of 222.4 ± 2.4 Ma within uncertainty. The $\varepsilon_{\text{Nd}}(t)$ values of hingganite-[Y] and xenotime were calculated using an age of 223 Ma, and range from −13.2 to −12.0 and −13.3 to −11.4, respectively (Fig. 2f). Bulk rock Sm-Nd isotope analyses of the lower Carboniferous red sandstone yielded ^{143}Nd/^{147}Nd values ranging from 0.511747 to 0.512008 (Table S-5). Initial $\varepsilon_{\text{Nd}}(t)$ values were calculated using the formation ages of 323 Ma for the red sandstone, ranging from −14.5 to −10.8 (Fig. 2f).

Discussion

Source of rare earths and uranium. This contribution focuses on the genesis of the HREE and U mineralisation of the Yushui Cu deposit. The new combined radioisotopic data from multiple minerals provide a consistent dataset with a concordant mineral formation age of *ca.* 223 ± 1 Ma. This age corresponds to a period of significant post-orogenic extension of the South China block (Zhao *et al.*, 2018). There is no magmatism at Yushui coeval with HREE and U mineralisation.

The $\varepsilon_{\text{Nd}}(t)$ values (−13.3 to −11.4) of HREE minerals from the unconformity at Yushui are consistent with those (−14.8 to −10.8) of the underlying red sandstone. Abundant detrital heavy minerals such as xenotime, monazite, rutile, and zircon occur in the footwall red sandstone sequence. These minerals show dissolution and alteration textures (Fig. S-7), which indicate fluid leaching of HREEs and U. This is also supported by the Y, Yb, and U distributions revealed by EPMA elemental mapping of xenotime in the red sandstone (Fig. 3).

Genetic links between unconformity-related U deposits and HREE mineralisation have been proposed elsewhere, for example in the Northern Territory, Australia (Nazari-Dehkordi *et al.*, 2018; Richter *et al.*, 2018), and the Athabasca Basin, Saskatchewan, Canada (Quirt *et al.*, 1991; Fayek and Kyser, 1997). Both these examples formed in extensional settings *via* the large scale circulation of oxidised, relatively low temperature saline fluids, with ore deposition taking place at redox interfaces (Quirt *et al.*, 1991; Fayek and Kyser, 1997; Nazari-Dehkordi *et al.*, 2018; Richter *et al.*, 2018). Similar fluids have been identified in primary fluid inclusions at Yushui (*i.e.* 8–15 wt. % NaCl equiv., 110–287 °C; Jiang *et al.*, 2016). In general, the hydrothermal transport of REEs requires complexation with a dominance of Cl^-, CO_3^{2-}, and SO_4^{2-} species (Williams-Jones *et al.*, 2012; Migdisov *et al.*, 2016; Zhou *et al.*, 2016). The occurrence of hydrothermal barite, anhydrite, hematite, synchysite-[Y], kamphaugite-[Y], and iimoriite-[Y] in the Yushui mineralisation indicates that the ore fluids were oxidised with a dominance of CO_3^{2-} and SO_4^{2-}. However, although redox reactions cannot effectively drive the formation of HREE-bearing minerals (Migdisov *et al.*, 2016), the presence of phosphorus in hydrothermal fluids can significantly lower the solubilities of HREEs (Williams-Jones *et al.*, 2012; Gysi *et al.*, 2015), and, notably, there are apatite-rich beds in the lower part of the overlying dolostone/limestone at Yushui. Therefore, we suggest that HREEs and U were leached from detrital minerals in the underlying hematite-bearing red sandstone by saline, oxidised basinal fluids

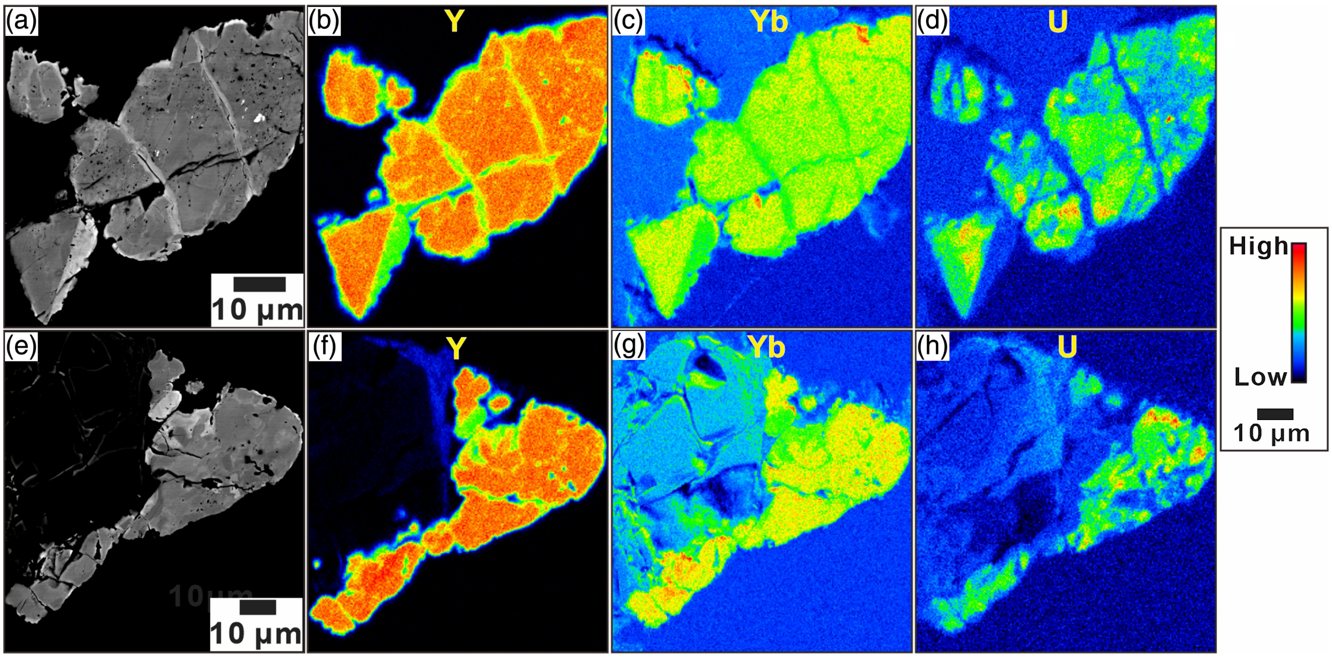

Figure 3 **(a, e)** Backscattered electron (BSE) images and electron probe microanalysis (EPMA) element maps of clastic xenotime in red sandstone, showing the distributions and textures of leaching of **(b, f)** Y, **(c, g)** Yb, and **(d, h)** U.

and were then precipitated in organic-rich beds in the overlying dolostone/limestone, which acted as a reductant and also provided P for efficient REE fixation.

Metal Endowment from the Final Assembly of Gondwana

The age range of 228–218 Ma for xenotime-I from the footwall red sandstone is coeval with the formation age (223 Ma) of HREE- and U-bearing minerals from the bedded mineralisation. The 387–329 Ma range for xenotime-II is comparable to the formation age of the Late Devonian to early Carboniferous sedimentary sequence. By contrast, the 486–404 Ma age range for detrital xenotime-III is coincident with the principal age peak at 470–410 Ma of detrital zircon in the footwall sandstone. The Devonian to Carboniferous successions in the South China block are dominated by siliciclastic units with minor coeval magmatism (Wang *et al.*, 2010), and contain significant amounts of detrital xenotime, monazite, rutile, and zircon. Triassic extension produced rifting-related, basinal fluid circulation and leaching of metals (*e.g.*, HREEs and U) by oxidised basinal fluids from the underlying red sandstone sequence. Notably, Late Devonian to early Carboniferous sedimentary red bed basins are found elsewhere (Song *et al.*, 2017), such as the Chu-Sarysu basin of Kazakhstan, which also hosts major redox-controlled U deposits (Dahlkamp, 2009). Therefore, this finding strongly suggests that analogous Carboniferous red bed sedimentary basins in South China and elsewhere may also host HREE and U mineralisation.

Crucially, the principal peak (421.2 ± 2.6 Ma) of detrital xenotime corresponds to the age of Silurian S-type granites in South China (Zhao *et al.*, 2018), suggesting that the footwall sandstone is ultimately derived from Silurian S-type granites. Such granites in South China are mainly peraluminous two mica/garnet granites. They have been interpreted as a far field response to early Palaeozoic continental collision and then orogenic collapse events (Wang *et al.*, 2010) (Fig. 4a), which led to the South China block becoming accreted to the northern margin of East Gondwana leading to the final Gondwana assembly (Fig. 4b) (Cawood *et al.*, 2013; Zhao *et al.*, 2018).

S-type granites generally have a metapelitic source characterised by accessory assemblages comprising xenotime, monazite, and zircon (Chappell *et al.*, 1987; Bea and Montero, 1999). Partial melting of metapelites can enhance the HREE and U concentrations in peraluminous melts (Bea and Montero, 1999; Villaseca *et al.*, 2003). In addition, P has a high solubility in strongly peraluminous S-type granitic magmas and there is substitution of $REE^{3+} + Y^{3+}$ for Zr ($ZrSiO_4 \leftrightarrow [REE,Y]PO_4$) in zircon from S-type granites which is charge balanced by P^{5+} (Burnham and Berry, 2017). Consequently, subsequent crystallisation of the S-type granites would produce abundant zircon, xenotime, and monazite.

The amalgamation of Gondwana is the most important period of S-type granite production in geological history, especially in Australia, Europe, and South China (Spencer *et al.*, 2014; Zhu *et al.*, 2020). Rapid erosion led to clastic sedimentary rocks that contain abundant HREE-U-bearing minerals which can then be leached by younger mineralising events. Furthermore,

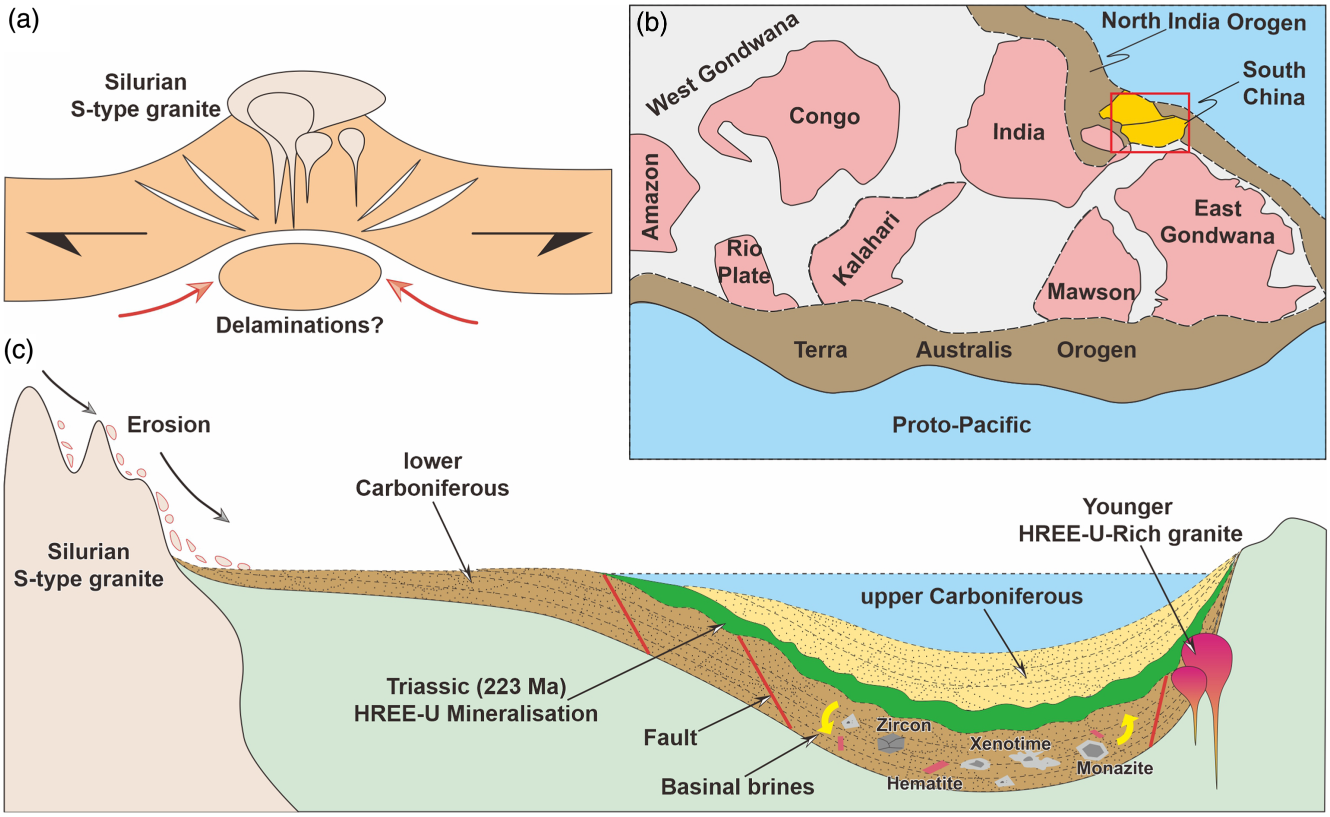

Figure 4 **(a)** Schematic genetic model of Silurian S-type granites as a far field response to early Palaeozoic continental collision and orogenic collapse events. **(b)** Schematic palaeogeographic reconstruction showing the position of the South China block during the Gondwana assembly (Cawood *et al.*, 2013). **(c)** Genetic model of erosion of Silurian S-type granites to form the lower Carboniferous red sandstone with abundant detrital zircon, xenotime, and monazite. Then Triassic extension allowed basinal fluid circulation, resulting in leaching of metals (*e.g.*, HREEs and U) from the red sandstone sequence.

these HREE-U-bearing clastic sedimentary rocks may undergo partial melting and generate younger HREE-U-rich granites (Fig. 4c) which may then be upgraded by processes in the critical zone to form the recent/subrecent regolith-hosted (or ion adsorption) HREE deposits of South China (Li *et al.*, 2017). Our study highlights that the final assembly of Gondwana established a long term metal reservoir in South China which was tapped repeatedly by ore forming fluids.

Acknowledgements

This research was jointly funded by the National Natural Science Foundation of China (Grants 42272070 and 42130102), the Young Star of Science and Technology Plan Projects in Shaanxi Province, China (Grant 2023KJXX-037) and the Natural Science Basic Research Program in Shaanxi Province of China (2022JC-DW5-01). PL is funded by the China Scholarship Council. SAG is funded by a Helmholtz Recruitment Initiative.

Editor: Raúl Fonseca

Additional Information

Supplementary Information accompanies this letter at https://www.geochemicalperspectivesletters.org/article2317.

Cite this letter as: Liu, P., Gleeson, S.A., Cook, N.J., Lehmann, B., Zhao, C., Yao, W., Bao, Z.A., Wu, S.T., Tian, Y.F., Mao, J.W. (2023) Final assembly of Gondwana enhances crustal metal (HREE and U) endowment. *Geochem. Persp. Let.* 26, 7–13. https://doi.org/10.7185/geochemlet.2317

References

Bea, F., Montero, P. (1999) Behavior of accessory phases and redistribution of Zr, REE, Y, Th, and U during metamorphism and partial melting of metapelites in the lower crust: an example from the Kinzigite Formation of Ivrea-Verbano, NW Italy. *Geochimica et Cosmochimica Acta* 63, 1133–1153. https://doi.org/10.1016/S0016-7037(98)00292-0

Burnham, A.D., Berry, A.J. (2017) Formation of Hadean granites by melting of igneous crust. *Nature Geoscience* 10, 457–461. https://doi.org/10.1038/ngeo2942

Cawood, P.A., Hawkesworth, C.J. (2015) Temporal relations between mineral deposits and global tectonic cycles. In: Jenkin, G.R.T., Lusty, P.A.J., Mcdonald, I., Smith, M.P., Boyce, A.J., Wilkinson, J.J. (Eds.) *Ore Deposits in an Evolving Earth*. Geological Society, London, Special Publication 393, Geological Society of London, 9–21. https://doi.org/10.1144/SP393.1

Cawood, P.A., Wang, Y., Xu, Y., Zhao, G. (2013) Locating South China in Rodinia and Gondwana: A fragment of greater India lithosphere? *Geology* 41, 903–906. https://doi.org/10.1130/G34395.1

Chappell, B.W., White, A.J.R., Wyborn, D. (1987) The Importance of Residual Source Material (Restite) in Granite Petrogenesis. *Journal of Petrology* 28, 1111–1138. https://doi.org/10.1093/petrology/28.6.1111

Dahlkamp, F.J. (2009) *Uranium Deposits of the World: Asia*. Springer-Verlag, Berlin, Heidelberg. https://doi.org/10.1007/978-3-540-78558-3

Fayek, M., Kyser, T.K. (1997) Characterization of multiple fluid-flow events and rare-earth-element mobility associated with formation of unconformity-type uranium deposits in the Athabasca Basin, Saskatchewan. *The Canadian Mineralogist* 35, 627–658. https://pubs.geoscienceworld.org/canmin/article-pdf/35/3/627/3420516/627.pdf

Gysi, A.P., Williams-Jones, A.E., Harlov, D. (2015) The solubility of xenotime-(Y) and other HREE phosphates ($DyPO_4$, $ErPO_4$, and $YbPO_4$) in aqueous solutions from 100 to 250 °C and p_{sat}. *Chemical Geology* 401, 83–95. https://doi.org/10.1016/j.chemgeo.2015.02.023

Hitzman, M., Kirkham, R., Broughton, D., Thorson, J., Selley, D. (2005) The Sediment-Hosted Stratiform Copper Ore System. In: Hedenquist, J.W., Thompson, J.F.H., Goldfarb, R.J., Richards, J.P. (Eds.) *Economic Geology One Hundreth Anniversary Volume*, Society of Economic Geologists, Inc., Littleton, Colorado, 609–642. https://doi.org/10.5382/AV100.19

Jiang, B.-b., Zhu, X.-y., Cheng, X.-y., Wang, H. (2016) Characteristics and geological significance of fluid inclusions in the Yushui copper polymetallic deposit, Guangdong Province. *Geology in China* 43, 2163–2172 (in Chinese with English abstract). http://doi.org/10.12029/gc20160624

Kositcin, N., McNaughton, N.J., Griffin, B.J., Fletcher, I.R., Groves, D.I., Rasmussen, B. (2003) Textural and geochemical discrimination between xenotime of different origin in the Archaean Witwatersrand Basin, South Africa. *Geochimica et Cosmochimica Acta* 67, 709–731. https://doi.org/10.1016/S0016-7037(02)01169-9

Košler, J., Fonneland, H., Sylvester, P., Tubrett, M., Pedersen, R.-B. (2002) U–Pb dating of detrital zircons for sediment provenance studies–a comparison of laser ablation ICPMS and SIMS techniques. *Chemical Geology* 182, 605–618. https://doi.org/10.1016/S0009-2541(01)00341-2

Li, Y.H.M., Zhao, W.W., Zhou, M.-F. (2017) Nature of parent rocks, mineralization styles and ore genesis of regolith-hosted REE deposits in South China: An integrated genetic model. *Journal of Asian Earth Sciences* 148, 65–95. https://doi.org/10.1016/j.jseaes.2017.08.004

Liu, P., Gu, X., Zhang, W., Hu, H., Chen, X., Wang, X., Song, W., Yu, M., Cook, N.J. (2023) Jingwenite-(Y) from the Yushui Cu deposit, South China: The first occurrence of a V-HREE-bearing silicate mineral. *American Mineralogist* 108, 192–196. https://doi.org/10.2138/am-2022-8373

McNaughton, N.J., Rasmussen, B., Fletcher, I.R. (1999) SHRIMP Uranium-Lead Dating of Diagenetic Xenotime in Siliciclastic Sedimentary Rocks. *Science* 285, 78–80. https://doi.org/10.1126/science.285.5424.78

Migdisov, A., Williams-Jones, A.E., Brugger, J., Caporuscio, F.A. (2016) Hydrothermal transport, deposition, and fractionation of the REE: Experimental data and thermodynamic calculations. *Chemical Geology* 439, 13–42. https://doi.org/10.1016/j.chemgeo.2016.06.005

Nazari-Dehkordi, T., Spandler, C., Oliver, N.H.S., Wilson, R. (2018) Unconformity-Related Rare Earth Element Deposits: A Regional-Scale Hydrothermal Mineralization Type of Northern Australia. *Economic Geology* 113, 1297–1305. https://doi.org/10.5382/econgeo.2018.4592

Quirt, D.H., Kotzer, T., Kyser, T.K. (1991) Tourmaline, phosphate minerals, zircon, and pitchblende in the Athabasca Group: Maw Zone and McArthur River areas, Saskatchewan. In: *Summary of Investigations 1991*. Saskatchewan Geological Survey, Saskatchewan Ministry of Energy and Mines, Miscellaneous Report 91-4, 181–191. https://pubsaskdev.blob.core.windows.net/pubsask-prod/88108/88108-Quirt-Kotzer-Kyser_1991_MiscRep91-4.pdf

Richter, L., Diamond, L.W., Atanasova, P., Banks, D.A., Gutzmer, J. (2018) Hydrothermal formation of heavy rare earth element (HREE)–xenotime deposits at 100 °C in a sedimentary basin. *Geology* 46, 263–266. https://doi.org/10.1130/G39871.1

Sawkins, F.J. (1984) *Metal Deposits in Relation to Plate Tectonics*. Springer, New York. https://doi.org/10.1007/978-3-642-96785-6

Song, H., Jiang, G., Poulton, S.W., Wignall, P.B., Tong, J., Song, H., An, Z., Chu, D., Tian, L., She, Z., Wang, C. (2017) The onset of widespread marine red beds and the evolution of ferruginous oceans. *Nature Communications* 8, 399. https://doi.org/10.1038/s41467-017-00502-x

Spencer, C.J., Cawood, P.A., Hawkesworth, C.J., Raub, T.D., Prave, A.R., Roberts, N.M.W. (2014) Proterozoic onset of crustal reworking and collisional tectonics: Reappraisal of the zircon oxygen isotope record. *Geology* 42, 451–454. https://doi.org/10.1130/G35363.1

Villaseca, C., Martín Romera, C., De la Rosa, J., Barbero, L. (2003) Residence and redistribution of REE, Y, Zr, Th and U during granulite-facies metamorphism: behaviour of accessory and major phases in peraluminous granulites of central Spain. *Chemical Geology* 200, 293–323. https://doi.org/10.1016/S0009-2541(03)00200-6

Wang, Y., Zhang, F., Fan, W., Zhang, G., Chen, S., Cawood, P.A., Zhang, A. (2010) Tectonic setting of the South China Block in the early Paleozoic: Resolving intracontinental and ocean closure models from detrital zircon U-Pb geochronology. *Tectonics* 29, TC6020. https://doi.org/10.1029/2010TC002750

Williams-Jones, A.E., Migdisov, A.A., Samson, I.M. (2012) Hydrothermal Mobilisation of the Rare Earth Elements – a Tale of "Ceria" and "Yttria". *Elements* 8, 355–360. https://doi.org/10.2113/gselements.8.5.355

Wu, S., Yang, M., Yang, Y., Xie, L., Huang, C., Wang, H., Yang, J. (2020) Improved *in situ* zircon U–Pb dating at high spatial resolution (5–16 μm) by laser ablation–single collector–sector field–ICP–MS using Jet sample and X skimmer cones. *International Journal of Mass Spectrometry* 456, 116394. https://doi.org/10.1016/j.ijms.2020.116394

Zhao, G., Wang, Y., Huang, B., Dong, Y., Li, S., Zhang, G., Yu, S. (2018) Geological reconstructions of the East Asian blocks: From the breakup of Rodinia to the assembly of Pangea. *Earth-Science Reviews* 186, 262–286. https://doi.org/10.1016/j.earscirev.2018.10.003

Zhou, L., Mavrogenes, J., Spandler, C., Li, H. (2016) A synthetic fluid inclusion study of the solubility of monazite-(La) and xenotime-(Y) in H_2O-Na-K-Cl-F-CO_2 fluids at 800 °C and 0.5 GPa. *Chemical Geology* 442, 121–129. https://doi.org/10.1016/j.chemgeo.2016.09.010

Zhu, Z., Campbell, I.H., Allen, C.M., Burnham, A.D. (2020) S-type granites: Their origin and distribution through time as determined from detrital zircons. *Earth and Planetary Science Letters* 536, 116140. https://doi.org/10.1016/j.epsl.2020.116140